Multiple photon excitation and ionization of NO in and on helium droplets

E. Polyakova
Department of Chemistry, Columbia University, New York, New York 10027

D. Stolyarov
Department of Physics, Brookhaven National Laboratory, Upton, New York 11973

C. Wittig[a)]
Department of Chemistry, University of Southern California, Los Angeles, California 90089

The photoexcitation of NO embedded in superfluid He_n nanodroplets having $\langle n \rangle \sim 10^4$ has been examined. Two-photon excitation prepares electronically excited states (NO^*), most notably, the embedded analog of the $A\,^2\Sigma$ state of gas phase NO. Vertical excitation to this low Rydberg state is blueshifted and broadened relative to its gas phase counterpart because of the repulsive electron-helium interaction. Transport to the droplet surface is believed to be facile in the superfluid. For example, NO^* prefers (energetically) to reside at the droplet surface rather than at the droplet center, in contrast to NO. Photoionization of surface-bound NO^* occurs over a significant photon energy range. This yields small cluster ions NO^+He_k, with $\sim 90\%$ of these clusters having $k \leq 10$. The variation of ion yield with photon energy displays a precipitous change in the region of $24\,300-24\,400$ cm^{-1} for all values of k. Possible photoionization mechanisms are discussed and it is suggested that intermediate levels with high-n Rydberg character play a role. This work underscores the important role played by transport in the photophysics of species embedded in the superfluid host. © *2006 American Institute of Physics*. [DOI: 10.1063/1.2198844]

I. INTRODUCTION

Interactions between neutral molecules/atoms and helium are among the weakest in nature, and those that involve liquid helium in its superfluid phase are particularly fascinating. The strengths and natures of such interactions can be interrogated by means of optical spectroscopies, e.g., shifts and widths of transitions can serve as sensitive probes. In recent years, the discovery of the essentially universal capacity of large helium clusters (also called droplets or nanodroplets) to pick up atoms and molecules (dopants) has spawned new vistas in helium-dopant spectroscopy.

Following the pioneering work of Hartmann *et al.*,[1] many experimental studies have been devoted to rovibronic spectroscopy of neutral molecules and van der Waals (vdW) complexes, including metastable complexes, in helium droplets.[2–4] Studies carried out in the infrared suggest that helium droplets might be considered the ultimate weakly interacting spectroscopic matrix. For example, shifts of vibrational origins are usually less than 0.1%.[3]

Whereas influences of helium on low-lying rovibrational excitations are modest, atomic and molecular electronic excitations can result in significant changes in interaction potentials. These derive from helium's sensitivity to electron density. Thus, photoexcitation can result in a profound rearrangement of the neighboring helium[5] and this can involve efficient coupling of molecular internal degrees of freedom to those of the helium host.[6]

When a small positive ion is embedded in helium, the attraction between the ion and the helium leads to condensation of helium near the ion. For example, mobility studies of liquid helium carried out in the 1970s have shown that helium forms a "snowball" around the positive ion. This snowball typically contains 30–50 atoms and has a diameter of ~ 12 Å.[7] In a model introduced by Lehmann and Northby,[8] helium of the droplet is considered as a dielectric liquid medium, and it is found that due to induction forces, positive ions are localized near the center. The trapping potential is found to be nearly harmonic in the vicinity of the equilibrium position, with a root mean squared thermal displacement of a few angstroms. Other theoretical studies have predicted the formation of a solidlike first shell around a positively charged center inside helium.[9]

Helium and electron density avoid one another because of Pauli repulsion. When placed in liquid helium, an electron displaces the helium and forms a "bubble," i.e., a spherical cavity with a diameter of 34 Å at zero pressure.[10,11] The creation of such a bubble requires ~ 0.8 eV, which is due to the reorganization energy of the bubble and the kinetic energy of the electron (i.e., due to its confinement). This is why—when it is brought close to a helium-vacuum interface—an electron does not penetrate into the bulk. Instead, due to long-range attractive forces, it attaches to the surface. The balance between short-range Pauli repulsion and long-range attraction causes a rearrangement of the helium close to the surface that results in the formation of a structure called a dimple.[5] A dimple is energetically more favorable than a bubble because the electron in a dimple is looser and the increase of the surface energy is smaller.

Effects that are due to a droplet's finite size cannot be

---

a)Electronic mail: wittig@usc.edu

124, 214308-1

ignored. The average droplet diameter in the present work is $\sim$100 Å. The helium density in the middle of the droplet is close to that of bulk helium. Calculations show that the thickness of the surface region where the density drops from 90% to 10% is $\sim$6 Å. Thus, $\sim$30% of the droplet volume belongs to the surface region, which is characterized by a significant density gradient.

As the helium density is lowered, less energy is required for the formation of an electron bubble. Thus, there is a force acting on a bubble formed in the region of the surface that pushes it toward the surface. Indeed, Farnik *et al.* have shown that an electron bubble is unstable in droplets smaller than 10^5 atoms.[10]

A. Embedded and surface-bound species

The two examples discussed above, i.e., of an electron and of a positively charged ion embedded inside a helium nanodroplet, show that the strength and nature of the helium-dopant interaction determines not just the configuration of the helium around the dopant, but whether the dopant resides within the droplet or on its surface.

The cases of an electron and a positively charged ion represent extreme situations. The solvation of a neutral species such as an atom or a molecule in a helium nanodroplet is more complex. Where a dopant resides—within the droplet versus on its surface—is determined by the balance between attractive induction and Pauli repulsion forces. This can be estimated with the model of Ancilotto *et al.*,[11] which compares the energy decrease due to the impurity-helium interaction to the energy increase due to creating a cavity in the helium. Referring to Eq. (1),[11] when the dimensionless parameter λ is less than 1.9, the dopant resides on the surface, whereas dopants with $\lambda > 1.9$ are solvated,

$$\lambda = 2^{-1/6}\frac{\rho \varepsilon r_e}{\sigma}, \qquad (1)$$

where ε is the well depth (in cm^{-1}) of the dopant-helium pair potential, σ is the surface tension (0.179 cm^{-1} Å^{-2}),[12] ρ is the density (0.022 Å^{-3}, with its gradient at the surface ignored),[13] and r_e is the equilibrium bond length (in angstroms) for the dopant-helium pair potential.

For most small closed-shell molecules, the well depth ε is between 50 and 100 cm^{-1}.[5] Experimental and theoretical studies have shown that the majority of molecules, van der Waals complexes, and nonmetallic atoms in their ground states reside within the droplet, rather than on its surface.[14] Equation (1) will be used later to show that ground state NO resides within the droplets.

In contrast, potentials for helium atoms interacting with alkali atoms are only slightly attractive; typically $\varepsilon < 1.5$ cm^{-1}. The shape of the helium surface around the alkali atom is determined by the interaction between the alkali atom outer electron and the helium. This can be described qualitatively by using the bubble model, though the bubble diameter is smaller than that of a free electron. Pursuant to this, alkali atoms and their clusters are believed to form dimple structures on the surface.[5]
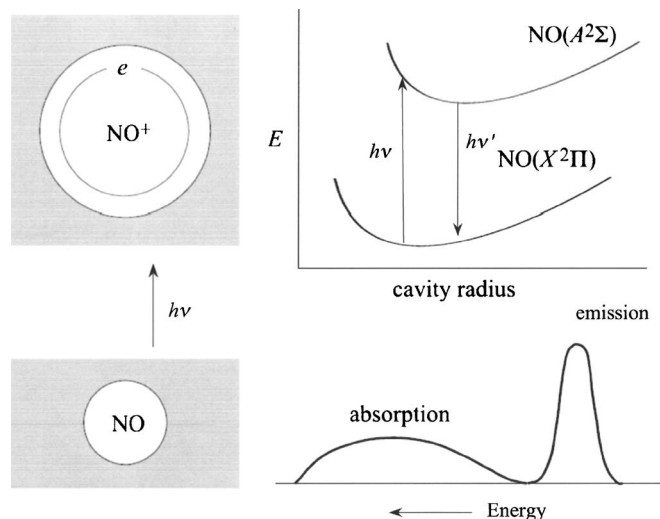

FIG. 1. Schematic illustration depicting the photoexcitation of NO from its ground state to a low-lying Rydberg state. Helium is represented by gray area. The Rydberg state (upper left) is shown with the helium in its relaxed state, i.e., the bottom of the excited state well shown as the NO($A\,^2\Sigma$) curve in the upper right. Following relaxation of the surrounding helium, emission takes place from the resulting bubble state, assuming that the excited state does not undergo relaxation by the helium.

Studies have been carried out on the spectroscopy of metal atoms in liquid helium. Because of Pauli repulsion between the helium and the extended electron densities of atom's electronically excited states, absorption lines are blueshifted by 500–1500 cm^{-1} relative to their gas phase values, and they have widths of 50–300 cm^{-1}.[5] Emission lines, on the other hand, are almost unshifted from their gas phase positions. This can be understood with the help of the scheme indicated in Fig. 1.[15] The potentials increase to the left of their equilibrium positions because of Pauli repulsion, and to the right because of the work required to create the void (bubble). The blueshift is due to the strong interaction of the extended orbital with the matrix environment, i.e., a Franck-Condon effect in which vertical excitation results in a state that is compressed relative to its equilibrium. On the other hand, emission from the relaxed excited state (i.e., the bottom of the upper well in Fig. 1) encounters no opposition from the helium. Namely, because the molecule-helium interaction for the electronically excited state is weak at the excited state equilibrium position, and even weaker for the dopant ground electronic state with the helium held at the excited state equilibrium position, the emission frequencies are close to those of the gas phase counterparts. Referring to Fig. 1, the emission spectrum lies near the gas phase emission photon energy. The energy of the *system* includes the work done to create the larger cavity, but this does not affect the emission frequency.

Evaluation of λ in Eq. (1) enables one to predict the manner in which a species is attached to a droplet, and this depends on the electronic state of the species. Thus, an electronic transition between ground and excited states (λ above and below 1.9, respectively) can initiate migration toward the droplet edge. Such expulsion upon electronic excitation has been observed experimentally. For example, He$_2(a\,^3\Sigma_u)$ has been examined in bulk helium and in droplets.[16–22] In
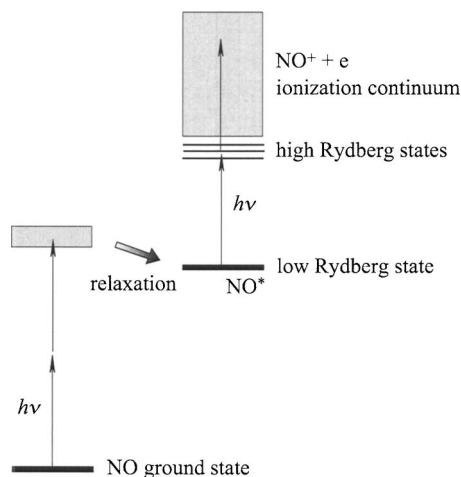
FIG. 2. Initial photoexcitation of NO is achieved via two-photon absorption, which places the system in a region of high potential energy. The helium experiences repulsion, and relaxation (thick arrow) follows on a picosecond time scale. Transport to the droplet surface results in a surface-bound low Rydberg state, NO*. This species can undergo photoexcitation via high Rydberg states to the ionization continuum.

bulk helium, He_2^* forms a 14 Å diameter bubble in which it freely rotates.[23] Whereas this bubble has a positive energy inside a droplet, He_2^* stays attached to the surface of the helium cluster in a weak potential and eventually detaches spontaneously.[24–26] Similarly, photoexcitation of a surface-bound alkali atom results in two processes: desorption and formation of He-alkali exciplexes followed by their detachment. Likewise, ground state Ag resides within the droplet, though with sufficient electronic excitation it is expelled.[27]

The above examples illustrate that guest-host interactions can change qualitatively when a species is promoted from its ground state to an electronically excited state. This is germane to the current study, in which embedded NO is excited to a low Rydberg level that moves to the droplet surface, where it then resides and is available for further photoexcitation, including ionization.

B. Photoexcitation and transport

This paper is focused on photoexcitation and intracluster transport processes that take place in clusters that contain a single embedded NO molecule. The schematic diagram in Fig. 2 illustrates the salient features. The idea is to start with ground state NO embedded in droplets of ~10^4 atoms. Photoexcitation is used to prepare a low Rydberg level of NO whose initial compressed confinement in the helium host relaxes on a picosecond time scale to form a bubble that makes its way to the droplet surface. It resides there, bathed in intense radiation that can induce further excitation and ionization.

Because of their large orbital radii, Rydberg levels are sensitive probes of local environment within the cluster and on its surface. The surface-bound low Rydberg level undergoes photoexcitation that ultimately results in ionization. Initial photoexcitation of embedded NO takes place via two-photon absorption, and subsequent excitation of the surface-bound low Rydberg level can proceed either resonantly or nonresonantly.
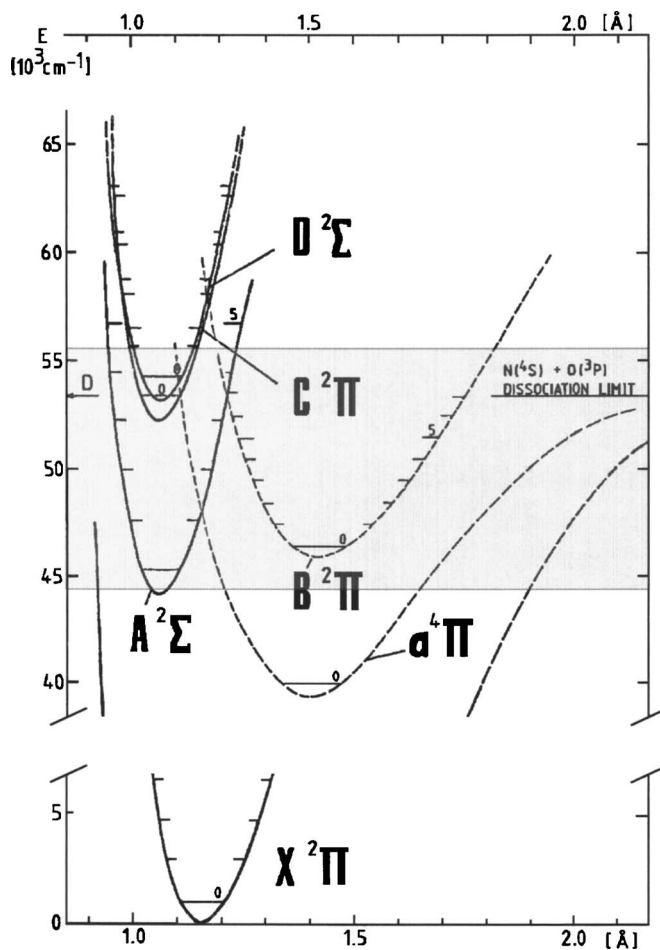

FIG. 3. Potential curves for NO showing low-lying electronic states. The spectral region used in the current study is shaded.

C. Electronically excited NO in host environments

NO has low Rydberg states due to its low ionization potential (74 721.67 cm^{-1}).[28] It has been studied in detail,[29] and absorption and fluorescence spectra are available for rare gas,[30–32] H_2,[33] and D_2 (Ref. 15) matrices. Its ground state electron configuration is

$$\cdots(2p\sigma)^2(2p\pi)^4(2p\pi^*)^1(2p\sigma^*)^0. \tag{2}$$

The low Rydberg states, $A\,^2\Sigma$, $C\,^2\Pi$, and $D\,^2\Sigma$, are obtained by promoting the $2p\pi^*$ electron to $3s\sigma$, $3p\pi$, and $3p\sigma$, respectively. Figure 3 shows potentials in the region of 40 000–60 000 cm^{-1}. In our experiments, NO is excited to energies in this range. The Rydberg states are easily ionized to yield ground state ions by one-electron excitation, e.g., for $A\,^2\Sigma$, the $3s\sigma$ electron is ejected,

$$(2p\sigma)^2(2p\pi)^4(2p\pi^*)^0(3s\sigma)^1 \rightarrow (2p\sigma)^2(2p\pi)^4(2p\pi^*)^0 + e^-. \tag{3}$$
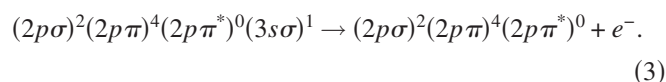
Because their bond lengths have values that are close to one another, there is a propensity for the ground electronic state of the ion to be formed in the same vibrational state as its Rydberg precursor, with the photoelectron acquiring the rest of the energy.[29] One or two photons are required for the ionization step.

TABLE I. Gas-matrix spectral shifts and widths for the lowest Rydberg state, $A\,^2\Sigma(v=0)$. The hosts are all solids (Refs. 31–34).

Host	Gas-matrix shift (eV)	FWHM (eV)
H_2	0.6	0.24
D_2	0.73	0.24
Ne	0.8	0.18
Ar	0.6	0.12
Kr	0.62	0.12
Xe	0.32	0.08

Referring to Fig. 3, in addition to the $A\,^2\Sigma$, $C\,^2\Pi$, and $D\,^2\Sigma$ states, the $B\,^2\Pi$ and $a\,^4\Pi$ valence states lie in this energy region. The transition $a\,^4\Pi \leftarrow X\,^2\Pi$ is spin forbidden, and $B\,^2\Pi(v') \leftarrow X\,^2\Pi(v''=0)$ is weak for $v' \leq 4$ due to small Franck-Condon factors.[34] Moreover, the $B\,^2\Pi$ ionization cross section for producing the ground state ion is significantly lower than that of $A\,^2\Sigma$ because it involves two-electron excitation,[35]

$$(2p\sigma)^2(2p\pi)^3(2p\pi^*)^2 \rightarrow (2p\sigma)^2(2p\pi)^4(2p\pi^*)^0 + e^-. \quad (4)$$

Though direct contributions to photoionization from valence states are negligible, $B\,^2\Pi$ and $a\,^4\Pi$ are believed to play roles in Rydberg-valence dynamics.[32]

The lowest Rydberg level, $A\,^2\Sigma$, is nearly spherical. Its electron density peaks ~ 3 Å from the NO center of mass and a tail extends to 5 Å.[36] Its vibrational levels in the region of 45 000–50 000 cm^{-1} are isolated from those of the valence states.

As mentioned above, the dynamics of electronic excitations in matrices has been studied.[37,38] Photoexcitation from the ground state results in overlap of the excited state electron density with the helium, inducing cage expansion and bubble formation.[38,39] An important point is that this spectrum can be simulated using the constants of free NO.

For example, in matrices, the $A\,^2\Sigma \leftarrow X\,^2\Pi$ vibrational bands are broadened (700–2000 cm^{-1}) and blueshifted (3500–7000 cm^{-1}) due to interactions of the extended orbital with the matrix. This phenomenon is general; Table I provides data for a number of host matrices. On the other hand, emission lines are narrower (500–650 cm^{-1}), and the line positions are close to their corresponding gas phase values, because the cage is smaller for the ground state than the excited state, as pointed out in the discussion relating to Fig. 1. Following cage expansion, the system can relax on a nanosecond time scale by radiation-less population transfer from $A\,^2\Sigma$ to $B\,^2\Pi$ and $a\,^4\Pi$. Coupling strengths for particular states depend strongly on the host matrix.

To conclude this section, consider NO–rare gas (RG) binary complexes for ground and Rydberg states of NO. This provides qualitative guidance concerning whether NO is inside the droplet or attached to the surface. Though spectroscopic data are not available for the ground electronic state of NO–He, theoretical studies indicate a T-shaped geometry bound by about 7 cm^{-1}, with values for ε and r_e of ~ 25 cm^{-1} and ~ 3.3 Å, respectively.[40] Substituting these values into Eq. (1) yields $\lambda = 11.3$, confirming that ground state NO lies within the droplet.
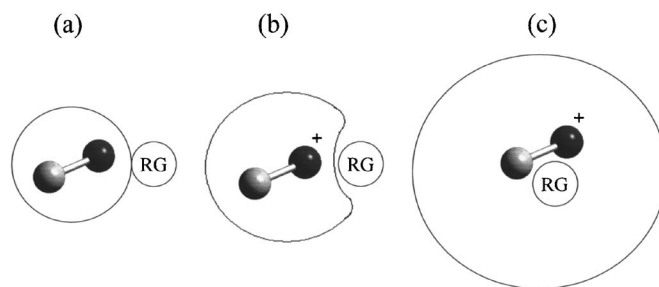

FIG. 4. (a) The lowest NO Rydberg level ($A\,^2\Pi$) interacts weakly with a rare gas atom. The Rydberg electron shields the core sufficiently that there is essentially no penetration of the rare gas atom. (b) Higher Rydberg levels can be intermediate; there is simultaneous shielding and penetration of the rare gas atom toward the positively charged core. (c) High Rydberg levels allow the rare gas atom to attach to the NO$^+$ core. The Rydberg electron density in the region of the core is modest.

Neither experimental nor theoretical studies of electronically excited NO–He are available. Wright and co-workers suggested that the $\widetilde{A}$ state of the NO–He complex is weakly bound and most likely dissociative. This assumption is based on trends in the spectroscopy and bonding of the $\widetilde{A}$ state of NO-RG complexes.[41] In *ab initio* studies of NO$^+$He,[42–44] Wright and co-workers obtained $\varepsilon = 198$ cm^{-1}, $r_e = 2.78$ Å, and an angle of $\sim 80°$.

Figure 4 illustrates a progression for a single rare gas atom interacting with NO:[41] (a) the $A\,^2\Sigma$ lowest Rydberg level, in which the RG atom keeps its distance from the Rydberg electron; (b) an intermediate level, in which the electron density is extended further than in (a) and the RG atom shows an indication of being attracted toward the core; and (iii) a high Rydberg level, in which the RG atom binds to the NO$^+$ core, with the Rydberg electron well removed on average from the core region. The principles depicted here are applicable to NO in/on helium droplets.[34]

II. EXPERIMENT

The experimental arrangement is depicted schematically in Fig. 5. The vacuum system consists of four separately pumped chambers. From left to right, the droplet source is located in chamber I. The droplets are produced by the continuous expansion of helium (Spectra Gases, 99.9999%) through a 5 μm diameter nozzle attached with a copper braid to a closed cycle refrigerator (Advanced Research Systems). Before arriving at the nozzle, the helium is precooled by passage through a heat exchanger attached to another closed cycle refrigerator (CTI Cryogenics). This arrangement enables the nozzle temperature to be maintained at 14.5 K. Temperatures were measured by using a silicon diode sensor (Lakeshore, ±0.1 K). The helium pressure behind the nozzle was 50 bars. The mean size of the clusters produced under these conditions is $\langle n \rangle \sim 11\,000$.[45,46]

After passing through a 400 μm diameter skimmer, the droplets enter chamber II, where they pass through a 3 cm long pickup cell containing NO (Matheson, CP grade, 99%, used without purification) that is located 10 cm downstream from the nozzle. The background pressure of the second chamber was $\sim 10^{-7}$ mbar. At this pressure, the peak that corresponds to the NO dimmer barely appears in the mass
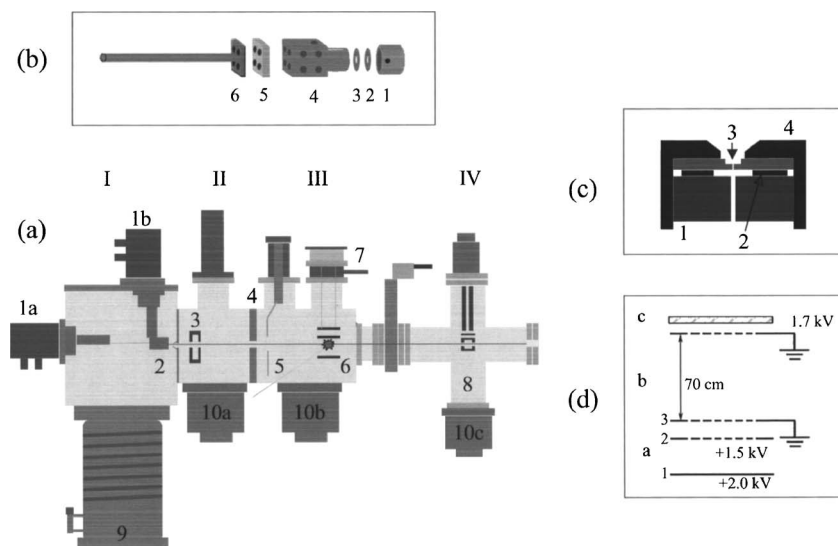
FIG. 5. Schematic of the experimental arrangement. (a) The machine consists of chambers I–IV: respectively, helium droplet source, pickup, detection, and quadrupole mass spectrometer. Other labels are 1a,b—closed cycle refrigerators; 2—nozzle; 3—pickup cell (more than one can be placed in series in chamber II); 4—cold finger; 5—copper plate; 6—set of electrodes; 7—microchannel plates; 8—quadrupole mass spectrometer; 9—diffusion pump; and 10a,b,c—turbomolecular pumps. In (b), the cooling assembly is shown. It consists of 1—brass nut, 2—copper disk with 5 μm aperture, 3—indium gasket, 4—copper nozzle body, 5—Teflon insulator, and 6—stainless steel nozzle mount. In (c), the nozzle assembly is shown. It consists of 1—copper nozzle body, 2—indium gasket, 3—copper disk with 5 μm aperture, and 4—brass nut. In (d), the electrode arrangement for the time-of-flight studies is shown: (a) electrode assembly: 1—repeller; 2—extractor; and 3—the ground shield; (b) TOF region; (c) microchannel plate.

spectrum recorded with the quadrupole mass spectrometer in chamber IV. Thus, most of the signal originates from droplets that contain a single NO molecule. This pressure was maintained during all measurements, except in an experiment in which the pressure dependence was recorded.

After leaving chamber II, the beam enters chamber III, which is pumped separately and is separated from chamber II by a 5 mm diameter diaphragm. To minimize the diffusion of gaseous NO into the detection region, a cold copper plate (labeled 5) was introduced; it is connected with a copper braid to a cold finger cooled by liquid nitrogen.

The ion detection arrangement is shown in the box labeled (d). It consists of (a) a set of electrodes, (b) a 75 cm long field-free time-of-flight region, and (c) the microchannel plate (MCP) ion detector (BURLE Electro-Optics). There are three electrodes: (1) repeller, (2) extractor, and (3) the ground shield. The repeller electrode is a round stainless steel plate 7.5 cm in diameter, while extractor and shield electrodes have 5 cm diameter fine nickel meshes in their centers. The spacing between the repeller and extractor electrodes is 1.25 cm, and the spacing between the extractor and shield electrodes is 0.625 cm. Voltages of 2.0 and 1.5 kV were applied to the repeller and extractor electrodes respectively. These voltages were optimized to provide the best mass resolution in the time-of-flight (TOF) spectra, i.e., to make the peak corresponding to NO$^+$, formed by photoionization of the trace amount of the background NO that is present in the chamber, as narrow as possible.

The radiation source was a dye laser equipped with an UV extension unit, as described elsewhere.[6] Briefly, the second harmonic of a Nd:YAG (yttrium aluminum garnet) laser (Continuum Powerlite 9020) pumped a dye laser (Continuum ND 6000). The output of the dye laser was mixed with residual 1064 nm radiation from second harmonic generation in a nonlinear crystal inside the ultraviolet extension unit (Continuum UVT-3). To cover the entire spectral range, the following laser dyes were used: Fluorescein 548, Rhodamine 590, a mixture of Rhodamine 590 and Rhodamine 610, Rhodamine 610, a mixture of Rhodamine 610 and

Rhodamine 640, Rhodamine 640, DCM, LDS 698, LDS 722, LDS 750, LDS 751, and LDS 765. All dyes were from Exciton.

The laser beam, focused by a 50 cm lens, intercepted the helium droplet beam in the region between the repeller and extractor electrodes. It was found that the intensity of the ion current depends strongly on the beam profile as well as the accuracy of the lens position adjustment. The lens must be centered and positioned perpendicular to the propagation direction of the laser beam to make the focal spot as tight as possible.

The output of the MCP detector is connected to an analog-to-digital converter board installed in a computer that controls the experiment through a fast amplifier. This allows us to record a TOF spectrum with each laser firing. We added 2000 spectra together to achieve a good signal-to-noise (S/N) ratio. We also used fast Fourier transform (FFT) filtering to eliminate high frequency noise, and base line correction was used when measuring peak intensities. At each wavelength a background TOF spectrum was recorded (i.e., with the helium droplet beam off) and it was subtracted from the TOF spectrum obtained with helium droplet beam on. This minimized the influence of background NO.

III. RESULTS

The experimental arrangement described above was used to record TOF mass spectra following the photoionization of helium droplets that contain embedded NO. By adjusting the pickup cell pressure, it was straightforward to ensure that only an insignificant percentage of the doped clusters contained two or more NO molecules. These conditions were maintained throughout this study. Photon wave numbers were set at discrete values throughout the range: $22\,222 \leq h\nu \leq 27\,816$ cm^{-1} (360–450 nm), which corresponds to the two-photon excitation range: $44\,444 \leq 2h\nu \leq 55\,632$ cm^{-1} shown in Fig. 3.

A typical mass spectrum is shown in Fig. 6. The most intense peak corresponds to NO$^+$. Background NO from the pickup cell also leads to NO$^+$. This background is most abundant when the laser frequency matches a transition of
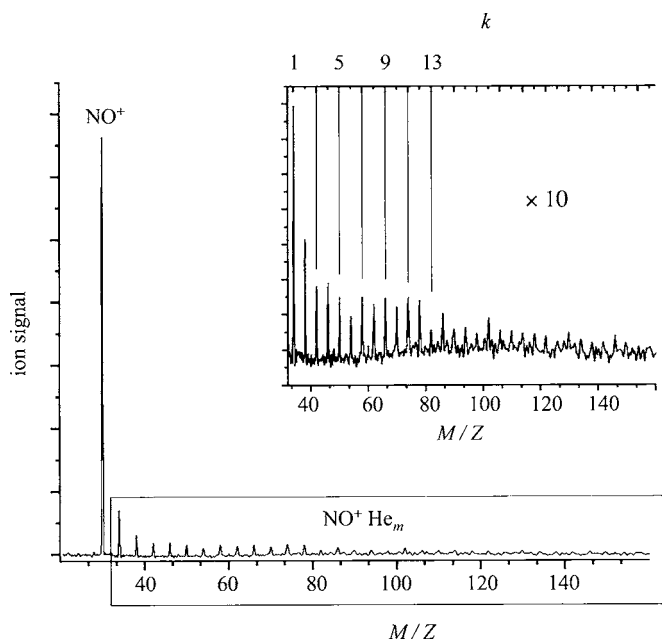
FIG. 6. Mass spectrum of ions formed by the irradiation ($h\nu$=24 330 cm^{-1}) of helium clusters containing embedded NO. The most intense peak corresponds to NO$^+$. The insert ($\times$10) shows the progression of NO$^+$He$_k$ clusters at masses of 34, 38, 42, etc.; the top axis indicates the number of helium atoms.
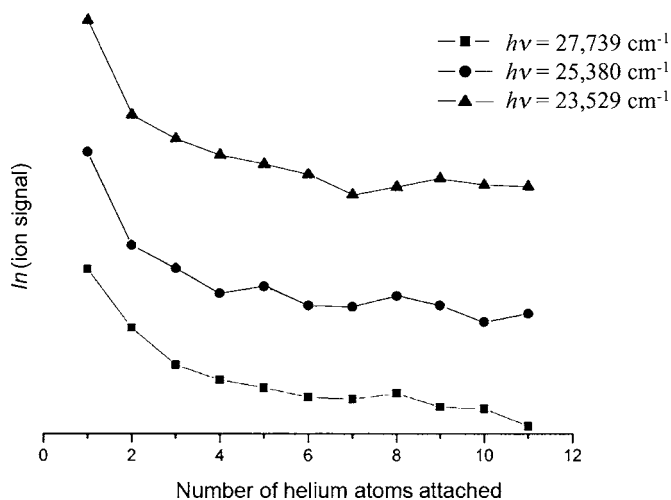

FIG. 7. Logarithmic plots of NO$^+$He$_k$ ion signal vs k. Data recorded at different values of $h\nu$ are displaced vertically for convenience. There is no essential difference between distributions obtained at different excitation energies.

gas phase NO. Because the gas phase line is sharp, it is easy to ensure that NO$^+$ signals are due mainly to the doped droplets. Namely, the transition frequencies of gas phase NO are simply avoided.

For each value of $h\nu$, a background TOF trace is recorded with the droplet beam off, and this trace is subtracted from the one obtained with the droplet beam on. In spectral regions well removed from the gas phase NO absorption features, more than 90% of the NO$^+$ ions derive from doped droplets. The weak gas phase background signal can be explained by near-resonant multiphoton ionization of NO.

Referring to Fig. 6, in addition to the NO$^+$ peak, there is a progression of peaks at masses given: $30+4k$, where k is an integer (see insert). The signal level is insignificant for k greater than 20. The $k \neq 0$ peaks are, of course, absent in the background spectrum. They are attributed to NO$^+$He$_k$ clusters, where k is the number of helium atoms attached to a NO$^+$ core. The intensity of the peaks decreases monotonically with k, with a relatively sharp decrease at 12 or 13. It is assumed that the intensity of a peak is related to the stability of its NO$^+$He$_k$ cluster. It has been found that for an atom or a small molecule about 12 atoms are required to form the first solvation shell.[36]

TOF spectra were recorded at 0.5 nm ($\sim$30 cm^{-1}) intervals throughout the region of 360–450 nm (22 222 $\leqslant h\nu$ $\leqslant$ 27 816 cm^{-1}). A total of 183 TOF spectra were recorded. No significant differences were observed in the distributions of peak height versus k.

Figure 7 presents logarithmic plots of distributions obtained at representative photon energies. Note that the distributions are essentially unchanged as $2h\nu$ changes by as much as 11 200 cm^{-1}. For gas phase NO, this range includes

a number of vibrational levels of the A $^2\Sigma^+$ state as well as ground vibrational levels of the C $^2\Pi$ and D $^2\Sigma$ states (Fig. 3).

Another way to view the data is to plot the variation of the ion signal at a given k vs $h\nu$. This was carried out for $0 \leqslant k \leqslant 9$. The results are presented in Fig. 8 for the range of 23 250–27 816 cm^{-1}. The entries are labeled according to the number of attached helium atoms. When $h\nu$ is less than 23 250 cm^{-1}, the NO$^+$He$_k$ ion signals are too weak to be reliable for k values exceeding 1, i.e., peaks are evident but the ability to record reliable relative peak heights is compromised. This is why the distributions shown in Fig. 8 are restricted to the range of 23 250–27 816 cm^{-1}. Only signals from NO$^+$ and NO$^+$He have been analyzed for the full range, 22 222–27 816 cm^{-1}.

Figure 9 shows a plot for NO$^+$He for the range of 22 222–27 816 cm^{-1}. This plot has the highest S/N ratio and it is not distorted by incomplete background subtraction. The inset covers the range of 24 185–24 445 cm^{-1}, recorded at a resolution of 1 cm^{-1}. In acquiring these data, results from 10 000 laser firings were averaged for each point, requiring 72 h. Because data were collected at 30 cm^{-1} intervals, such plots are not referred to as "spectra." The TOF spectra were recorded by averaging 2000 points each for signal and background traces. Thus, each TOF spectrum requires 7 min, and a data set requires 21 h. In practice it takes a week to record a data set, making it impractical to cover the range of 22 222–27 816 cm^{-1}. Resolution of 0.2 cm^{-1} would require approximately half a year.

One can see from Figs. 8 and 9 that some features are robust. The most prominent is the drop between 24 300 and 24 400 cm^{-1}. Others are peaks at $\sim$23 380, 24 000, and 24 300 cm^{-1}; the inset to Fig. 9 confirms the one at $\sim$24 300 cm^{-1}. Similar dependencies for producing NO$^+$ and (NO·He$_k$)$^+$ suggest a common mechanism. As opposed to absorption and emission spectra of NO in rare gases, H$_2$ and
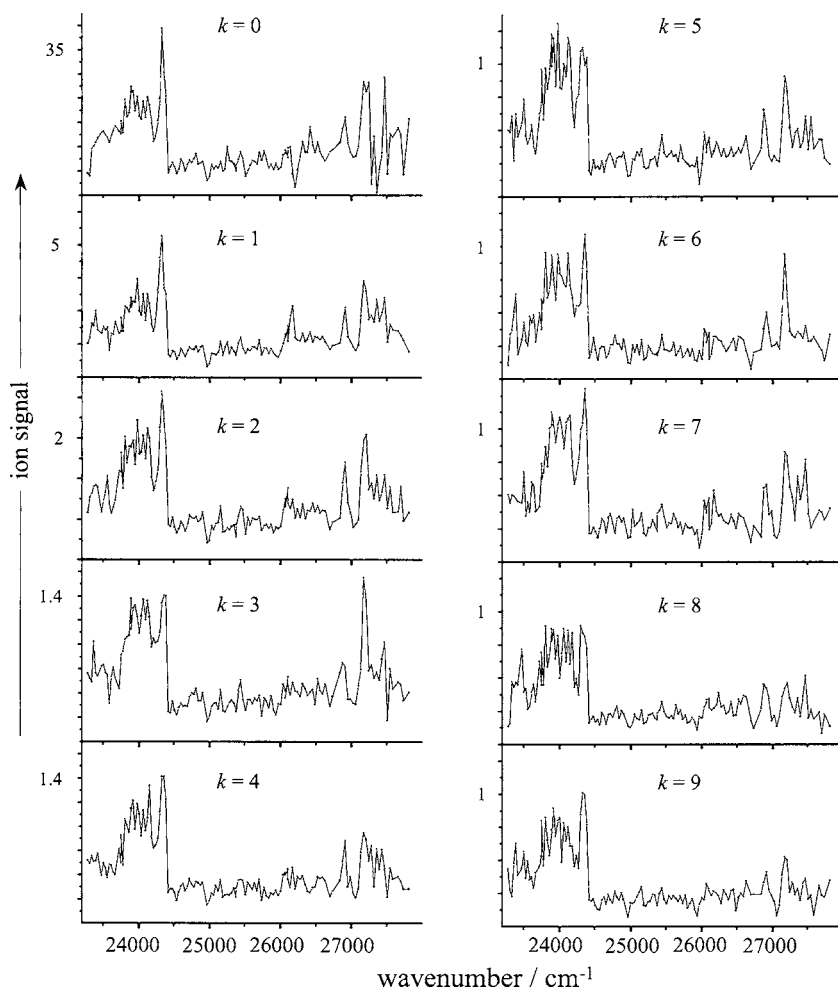
FIG. 8. NO⁺He_{k} ion signal vs $h\nu$ for different numbers of attached helium atoms, $0 \leq k \leq 9$. Data were recorded at $h\nu$ values separated by 30 cm^{-1}.

D_2 matrices, the wavelength dependencies in Figs. 8 and 9 cannot be reconstructed from the spectrum of the NO in a simple way. This suggests a NO⁺He_{k} formation mechanism that includes the droplet's superfluid nature.

IV. DISCUSSION

It is nontrivial that NO molecules embedded in helium droplets having $\langle n \rangle \sim 10^4$ are ionized via one or more mechanisms in which the first step is two-photon excitation of low-lying Rydberg intermediates. The overall process is complicated, subsuming phenomena that can, in principle, act in series and/or parallel: (i) two-photon excitation of low-lying Rydberg levels; (ii) subsequent relaxation of nuclear degrees of freedom in and between NO and the helium host; (iii) transport of electronically excited NO to the droplet surface; (iv) two-photon ionization of surface-bound electronically excited NO; (v) possible separation from the parent cluster of high Rydberg states, including a modest number of helium atoms carried along with the high Rydberg state; (vi) possible separation from the parent cluster of NO⁺He_{k} clusters; and (vii) stabilization of surface-bound high Rydberg states through snowball formation at the ion core. In interpreting the results, we shall focus on the most robust experimental observations.

A. Two-photon excitation of embedded NO

Two-photon excitation of embedded NO promotes it from its $X\,^2\Pi$ ground electronic state (referred to as the X state) to one or more low-lying Rydberg states. As pointed out earlier, a number of studies have been carried out to determine how low-energy electronically excited states of NO behave in rare gas and $H_2(D_2)$ matrices, where broadenings and blueshifts have been reported.[31–34] The lowest-energy Rydberg state of gaseous NO is $A\,^2\Sigma^+$ (referred to as the A state) which has been implicated as the major participant in the low-energy ultraviolet absorption features of NO in the host matrices.

There is no doubt that two-photon $A\,^2\Sigma^+ \leftarrow X\,^2\Pi$ photoexcitation promotes such systems to regimes of high potential energy (Figs. 1–3), from which the nuclear degrees of freedom relax to a relatively quiescent state. For example, following $A\,^2\Sigma^+(\nu=0) \leftarrow X\,^2\Pi$ photoexcitation in an argon matrix, the dominant A-state relaxation mechanism has been shown to be spontaneous emission from $A\,^2\Sigma^+(\nu=0)$.[32,41,47] In addition, depletion spectra have been recorded by promoting the A state to yet higher electronic levels while monitoring $A \rightarrow X$ spontaneous emission. These display Rydberg-type signatures, and assignments have been suggested up to the ionization limit, which is lower than for gas phase NO, i.e., 8.26 versus 9.26 eV, respectively.[41,48]

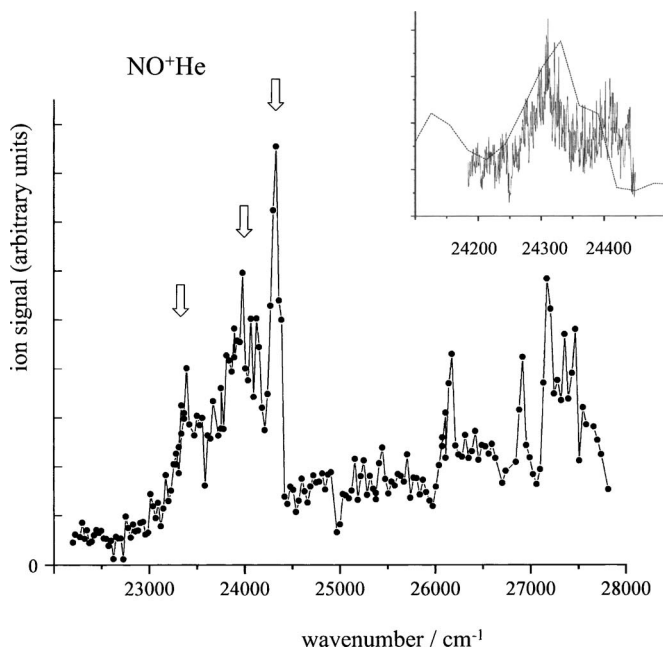Now consider two-photon $A \leftarrow X$ vertical excitation. This

FIG. 9. Mass spectrometer signal at $M/Z=34$ (i.e., NO^+He) vs $h\nu$; points are separated by 30 cm^{-1}. The arrows indicate peaks at 23 380, 24 000, and 24 300 cm^{-1} that we attribute to excitation of intermediate surface-bound high Rydberg states that facilitate photoionization. See text for details. Note the abrupt drop of the ion signal between 24 300 and 24 400 cm^{-1}. The insert shows data recorded at 1 cm^{-1} intervals, averaging results from 10 000 laser firings at each point. Data from the main trace are shown as a dashed line connecting the points separated by 30 cm^{-1}.

extends an electron into the helium (which it abhors), resulting in broadening and blueshift. Relaxation of the nuclear degrees of freedom of the combined dopant-host system ensues. The helium is pushed away to create a bubblelike state. The low-density liquid responds on a time scale of a few picoseconds, which is essentially instantaneous relative to that of subsequent transport of the electronically excited moiety through the droplet. The bubblelike state has a diameter of ~8 Å,[36] which is smaller than the 34 Å bubble of a free electron in helium.

The energy required for the lowest NO Rydberg level to create a void within the droplet is estimated by using the bubble model to be ~100 cm^{-1},[49] which is small relative to the corresponding energy for an electron in helium. The difference is due mainly to the void being smaller by a factor of ~4. Therefore, most of the energy that constitutes the blueshift in the absorption spectrum of NO in helium (thousands of cm^{-1}) will be dissipated as heat. Bubble formation causes evaporation until the low temperature environment recovers; the time scale is estimated to be <1 ns from the work of Stein.[50]

Unlike the argon host, the ionization of NO within bulk helium requires more energy than for the ionization of gas phase NO. An energy of ~1 eV is required to form the electron bubble, and less than that is gained by the solvation of NO^+ by helium. Thus, three-photon ionization is unlikely in the work reported here because the photons employed have insufficient energy.

B. Transport to the surface

The NO bubble prepared by two-photon absorption is present initially in the interior of the droplet. Hereafter, NO^* denotes the lowest Rydberg level of embedded NO, i.e., the counterpart to the $A\ ^2\Sigma^+$ state of gaseous NO. The NO^* bubble does not stand still, because (at the very least) of the zero-point excitation of NO confined to the region of the droplet center. Unlike NO, which resides in a shallow well whose minimum is at the droplet center, NO^* experiences no such attractive well. It experiences a potential that favors transport toward the surface.

In the superfluid regime, dopant transport is unimpeded over large distances. To illustrate the efficacy of bulk-to-surface transport, suppose NO^* has a speed of 10 m s^{-1}. To travel a straight-line distance of 30 Å requires only 300 ps, which is considerably smaller than the 10 ns laser pulse duration. Thus, we assume that on average the NO^* makes its way to the droplet surface quickly relative to the laser pulse duration. Moreover, the energy of the system is lower with NO^* at the surface than with NO^* embedded in the helium, providing a driving force for NO^* going to surface.

On the basis of the above, it is assumed that NO^* goes to the surface before undergoing photoexcitation. While resident there, it can be promoted to higher electronic states, from which it can be photoionized. The long laser pulse duration, relative to the mean transport time from the interior of a droplet to the surface, as well as the high energies of the laser pulses, ensure efficient photoexcitation of surface-bound NO^*.

Were NO^* photoionized *within* the droplet, the electron might leave. A high-energy electron can, in principle, leave quickly (femtoseconds), whereas degradation of the electron's kinetic energy will heat the helium. With sufficient deactivation, an electron can expand the helium that surrounds it to create a bubble. However, an electron bubble is not stable in droplets of the sizes used in the current studies, so it must either recombine with the positive ion or leave the cluster. With the former, the resulting excited states will probably be deexcited through interaction with the helium and/or spontaneous emission. The amount of available energy is so large that all of the helium can be evaporated in droplets with $n\sim10^4$. On the other hand, if an electron bubble escapes into vacuum it will be cold. For example, Peterka *et al.*, in examining the photoionization of undoped helium droplets, reported that the resulting electrons have almost zero velocity.[51] The formation of such slow electrons is consistent with the efficient dissipation of their nascent kinetic energies.

Where a NO^+ ion created (say, at $t=0$) deep within its cluster, with the electron quickly ejected from the cluster into vacuum, it is improbable that small clusters such as the ones presented in Figs. 6 and 7 would be produced. Phonons are created by the abrupt introduction of a nonequilibrium situation. Namely, the NO^* bubble precursor is of such a nature that the helium lies outside the volume occupied by its Rydberg electron. At $t=0$, NO^+ is created, which immediately begins to draw helium toward itself, with NO^+-He binding energies of ~200 cm^{-1} per He atom for the first solvation

shell. Evaporation follows. However, the amount of energy that goes into evaporation is small compared to that needed to create the electron-ion pair. For example, for $n = 10^4$, $\sim 50\,000$ cm^{-1} is needed to evaporate all of the helium. This is much larger than $4h\nu$ minus the energy needed to create a gas phase electron (with zero kinetic energy) and a solvated NO$^+$. Thus, it is expected that in this case large ionized clusters will be produced. We see no evidence of such large clusters. Referring to Fig. 7, the ion signal diminishes as the number of attached helium atoms increases, with the total number of clusters that have ten or fewer helium atoms accounting for $\sim 90\%$ of the ion signal.

Caveats not yet addressed experimentally are (i) the fact that large clusters might not yield ion signals efficiently upon impacting the MCP; and (ii) because of their large momentum along the molecular beam axis, they may miss the MCP detector. Referring to (i), upon impact at the MCP the translational energy of the NO$^+$ moiety is small, and the surrounding helium does not yield electrons. Rather, the surrounding helium behaves as a dense gas hitting the plate, with each helium atom having a small translational energy. Stienkemeier *et al.* have reported signals for large ionized helium droplets using MCP detectors.[52] Nonetheless, sensitivity to such large clusters remains an issue.

C. NO* at the surface

Consider NO* on the surface. As mentioned above, bulk-to-surface transport occurs on a shorter time scale than that of the laser pulse. It is suggested that photoionization is dominated by contributions from surface-bound NO* for two reasons: (i) NO* spends most of its time on the surface and (ii) it is easier to eject an electron from NO* into vacuum than into helium. It is assumed that the excitation rate brought about by the intense radiation is not so large that a significant percent of NO* is photoionized as it makes its way to the surface. This interesting regime can be approached with short-duration laser pulses.

Regardless of the details of the electronically excited states of surface-bound NO, we know that such states exist, the lowest being NO*. In the bulk, rather than attaching helium, NO* repels it, creating a bubble. For the surface-bound analog, the NO* electron density is larger outside the droplet than inside due to a trade-off. On the one hand the energy is raised in order to distort the electron density, while on the other hand the energy is lowered when the electron is kept away from the helium, which also makes the NO core more accessible to the helium. The trade-off is such that the electron lies more outside than inside the droplet.[53] It is assumed that NO* does not undergo significant electronic deactivation during the 10 ns laser pulse. Deactivation does not occur in argon matrices and there is no reason for it to be more efficient in helium.

Whereas NO* electronic excitation is robust, vibrational relaxation of the core is likely. Several vibrational levels of NO in the $A\,^2\Sigma^+$ state are accessible by two-photon excitation in the range of $22\,222 - 27\,816$ cm^{-1}. The vibrational quantum of the $A\,^2\Sigma^+$ state is 2374 cm^{-1}, which is sufficient to evaporate ~ 11 helium atoms from the first solvation shell,

as estimated from the NO$^+$–He binding energy. Therefore, one would expect the number of helium atoms in the snowball to decrease with vibrational excitation if NO carries vibrational excitation into the snowball. Figure 8 shows that this is not the case: the distribution of the number of helium atoms carried by NO$^+$ is independent of the photon energy. To the extent that NO$^+$ formed by ionization of NO* preserves vibrational excitation, our results indicate that the NO$^+$ core undergoes efficient vibrational relaxation before the snowball is formed.

Now consider high principle quantum numbers. As the Rydberg electron spends most of its time far from the core, it has no trouble avoiding helium condensed around the core. An image is that NO$^+$ lies within the droplet, and the electron is outside with only modest density penetrating the surface. Calculations by Golov and Sekatskii[53] have shown that such states are stable, though no experimental verification has been reported to date.

Thus, two limits have been identified: the lowest Rydberg level, NO*, in which helium is excluded from the region of the core, and high Rydberg levels, in which the electron is mainly outside NO$^+$He$_n$. There must exist a regime in which the system undergoes a transition between these limits. Recall Fig. 4, which depicts an analogous situation for a single rare gas atom. Though we do not know the details of this transition, we know it exists. Thus, it is instructive to consider likely consequences vis-à-vis photoionization.

First, consider photoionization of surface-bound NO*, in which an electron is ejected with no intermediate nuclear dynamics. Helium rushes toward NO$^+$ and the ensuing dynamics are vigorous, with concomitant boiling, evaporation, and condensation. The entire region has turned into a hot gas, with condensation restricted to the NO$^+$ seed, and relatively small NO$^+$He$_k$ clusters are formed. This scenario is appropriate if helium is kept away from the core in any intermediate step.

Recall that Figs. 8 and 9 show peaks near 23 380, 24 000, and 24 300 cm^{-1}. These cannot be assigned to vibrations because the peak-to-peak separations do not correspond to vibrational frequencies. They can be attributed to excitation of Rydberg levels starting from surface-bound NO*.

Now consider photoexcitation of surface-bound NO* in which a high Rydberg level is prepared whose core is weakly shielded by the Rydberg electron density. Helium can condense around the core because the Rydberg electron density near the NO$^+$ core is sufficiently small that a shell of helium around the NO$^+$ core adds little to the energy of the Rydberg electron. Once helium has condensed around NO$^+$, it will (for all practical purposes) be impossible to obtain small NO$^+$He$_k$ clusters of the kind shown in Fig. 6 by photoionizing the surface-bound high Rydberg level. The reason is that most of the agitation associated with condensing helium around NO$^+$ has already occurred.

The above considerations provide a rationalization for the drop in signal between 24 300 and 24 400 cm^{-1} shown in Figs. 8 and 9. When the photon energy is relatively low, ionization occurs via states that prevent helium from collecting at the core. As the photon energy increases, higher Rydberg levels with larger radii are excited. At some point,

Rydberg excitation is accompanied by condensation of helium around the NO$^+$ core. Removing the high Rydberg electron via photoionization results in modest agitation in the vicinity of the NO$^+$, but not enough to break up the cluster. This results in a pronounced drop in signal. This mechanism is a viable explanation of the precipitous drop in signal between 24 300 and 24 400 cm^{-1}.

To complete the discussion, consider the possibility that the step that produces the high Rydberg level involves fragmentation,

$$NO^*He_n + h\nu \rightarrow NO^{**}He_{k'} + He_{n'}, \tag{5}$$
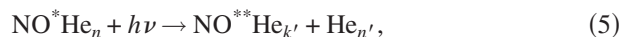
where ** denotes a high Rydberg level. If the parent cluster contains n helium atoms, then the inequality $k' + n' \leqslant n$ admits additional atomic and cluster fragments.

Consider now the fate of NO**He$_{k'}$. There is no reason to assume *a priori* that such electronic excitations are stable; perhaps they decay via nonadiabatic interaction. After all, the helium in the NO**He$_{k'}$ cluster is excited, unlike the helium in the parent cluster or the solid argon in argon matrices. Specifically, the NO**He$_{k'}$ cluster is formed via a vigorous process, and evaporation is not effective for small k' values, because the helium is strongly bound to the NO$^+$ core ($\sim$200 cm^{-1}/at.), unlike with large clusters, where evaporation requires just 5 cm^{-1}. Efficient nonadiabatic decay will inhibit photoionization. In other words, as the photon energy is increased, if reaction (5) eventually turns on, but with NO**He$_{k'}$ decaying via nonadiabatic interaction, the ionization signal will drop. This is consistent with the precipitous drop shown in Figs. 8 and 9.

On the other hand, if NO** electronic excitation is stable in NO**He$_{k'}$, this species will be efficiently photoionized, yielding NO$^+$He$_k$. This is consistent with the observation that the cluster size distribution is independent of the photon energy over a broad range. Namely, removal of the high Rydberg electron does not create much vibrational excitation in NO$^+$ because the bond lengths of NO** and NO$^+$ have essentially the same values. However, because this mechanism does not explain the drop, it is excluded.

V. CONCLUSION

Photoionization of NO in superfluid helium droplets has been examined. In contrast to rare gas matrices, superfluidity assures mobility. The overall process is complex, involving a number of phenomena: (i) two-photon excitation of low-lying Rydberg levels; (ii) subsequent relaxation of nuclear degrees of freedom in and between NO and the helium host; (iii) transport of NO* to the droplet surface; (iv) two-photon ionization via high Rydberg intermediates of surface-bound NO*; (v) possible separation from the parent cluster of high Rydberg states, including a modest number of helium atoms carried along with the high Rydberg state; (vi) possible separation from the parent cluster of NO$^+$He$_k$ clusters; and (vii) stabilization of surface-bound high Rydberg states through snowball formation at the ion core. It is concluded that NO* goes to the surface and is then photoionized, creating NO$^+$He$_k$ snowballs. Transport plays a major role in the photophysics.

[1] M. Hartmann, R. Miller, J. Toennies, and A. Vilesov, Phys. Rev. Lett. **75**, 1566 (1995).
[2] K. Nauta and R. E. Miller, Science **283**, 1895 (1999).
[3] C. Callegari, K. K. Lehmann, R. Schmied, and G. Scoles, J. Chem. Phys. **115**, 10090 (2001).
[4] K. Nauta and R. E. Miller, J. Chem. Phys. **113**, 10158 (2000).
[5] F. Stienkemeier and A. F. Vilesov, J. Chem. Phys. **115**, 10119 (2001).
[6] E. Polyakova, D. Stolyarov, X. Zhang, V. V. Kresin, and C. Wittig, Chem. Phys. Lett. **375**, 253 (2003).
[7] K. R. Atkins, Phys. Rev. **116**, 1339 (1959).
[8] K. K. Lehmann and J. A. Northby, Mol. Phys. **97**, 639 (1999).
[9] A. Nakayama and K. Yamashita, J. Chem. Phys. **112**, 10966 (2000).
[10] M. Farnik, B. Samelin, and J. P. Toennies, J. Chem. Phys. **110**, 9195 (1999).
[11] F. Ancilotto, P. B. Lerner, and M. W. Cole, J. Low Temp. Phys. **101**, 1123 (1995).
[12] R. Bowley, J. Phys. C **3**, 2012 (1970).
[13] J. P. Toennies and A. F. Vilesov, Angew. Chem., Int. Ed. **43**, 2622 (2004).
[14] J. P. Toennies and A. F. Vilesov, Annu. Rev. Phys. Chem. **49**, 1 (1998).
[15] F. Vigliotti, A. Cavina, C. Bressler, B. Lang, and M. Chergui, J. Chem. Phys. **116**, 4542 (2002).
[16] C. Surko and F. Reif, Phys. Rev. **175**, 229 (1968).
[17] K. von Haeften, A. R. B. de Castro, M. Joppien, L. Moussavizadeh, R. von Pietrowski, and T. Moller, Phys. Rev. Lett. **78**, 4371 (1997).
[18] K. von Haeften, T. Laarmann, H. Wabnitz, and T. Moller, Phys. Rev. Lett. **88**, 056101 (2002).
[19] K. von Haeften, T. Laarmann, H. Wabnitz, and T. Moller, J. Phys. B **38**, S373 (2005).
[20] A. V. Benderskii, R. Zadoyan, N. Schwentner, and V. A. Apkarian, J. Chem. Phys. **110**, 1542 (1999).
[21] S. Yurgenson, C.-C. Hu, C. Kim, and J. A. Northby, Eur. Phys. J. D **9**, 153 (1999).
[22] J. A. Northby, S. Yurgenson, and C. Kim, J. Low Temp. Phys. **101**, 427 (1995).
[23] J. Eloranta, N. Schwentner, and V. A. Apkarian, J. Chem. Phys. **116**, 4039 (2002).
[24] H. Buchenau, J. P. Toennies, and J. A. Northby, J. Chem. Phys. **95**, 8134 (1991).
[25] C. Kim, S. Yurgenson, C. C. Hu, and J. A. Northby, J. Low Temp. Phys. **113**, 1097 (1998).
[26] S. Curtis, A. Boatwright, R. R. Wright, and A. J. Stace, Chem. Phys. Lett. **401**, 254 (2005).
[27] F. Federmann, K. Hoffmann, N. Quaas, and J. D. Close, Phys. Rev. Lett. **83**, 2548 (1999).
[28] D. T. Biernacki, S. D. Colson, and E. E. Eyler, J. Chem. Phys. **89**, 2599 (1988).
[29] J. C. Miller and R. N. Compton, J. Chem. Phys. **84**, 675 (1986).
[30] M. Chergui, N. Schwentner, and W. Bohmer, J. Chem. Phys. **85**, 2472 (1986).
[31] M. Chergui and N. Schwentner, J. Chem. Phys. **97**, 2881 (1992).
[32] M. Chergui and N. Schwentner, J. Chem. Phys. **91**, 5993 (1989).
[33] F. Vigliotti, M. Chergui, M. Dickgiesser, and N. Schwentner, Faraday Discuss. **108**, 139 (1997).
[34] M. Chergui, R. Schriever, and N. Schwentner, J. Chem. Phys. **89**, 7083 (1988).
[35] H. Zacharias, F. deRougemont, T. F. Heinz, and M. M. T. Loy, J. Chem. Phys. **105**, 111 (1996).
[36] M. Gross and F. Spiegelmann, Eur. Phys. J. D **4**, 219 (1998).
[37] J. Eloranta, K. Vaskonen, H. Hakkanen, T. Kiljunen, and H. Kunttu, J. Chem. Phys. **109**, 7784 (1998).
[38] M. T. PortellaOberli, C. Jeannin, and M. Chergui, Chem. Phys. Lett. **259**, 475 (1996).
[39] G. Rojas-Lorenzo, J. Rubayo-Soneira, F. Vigliotti, and M. Chergui, Phys. Rev. B **67**, 115119 (2003).
[40] J. Klos, G. Chalasinski, M. T. Berry, R. Bukowski, and S. M. Cybulski, J.

Chem. Phys. **112**, 2195 (2000).

[41] J. D. Barr, J. M. Dyke, P. Mack, D. Smith, and T. G. Wright, J. Electron Spectrosc. Relat. Phenom. **97**, 159 (1998).

[42] E. P. F. Lee, P. Soldan, and T. G. Wright, J. Phys. Chem. A **102**, 6858 (1998).

[43] J. M. Robbe, M. Bencheikh, and J. P. Flament, Chem. Phys. Lett. **210**, 170 (1993).

[44] P. Soldan, E. P. F. Lee, and T. G. Wright, J. Chem. Phys. **116**, 2395 (2002).

[45] J. Harms, J. P. Toennies, and F. Dalfovo, Phys. Rev. B **58**, 3341 (1998).

[46] M. Lewerenz, B. Schilling, and J. P. Toennies, Chem. Phys. Lett. **206**, 381 (1993).

[47] F. Vigliotti, G. Zerza, M. Chergui, and J. Rubayo-Soneira, J. Chem. Phys. **109**, 3508 (1998).

[48] G. Zerza, F. Vigliotti, A. Sassara, M. Chergui, and V. Stepanenko, Chem. Phys. Lett. **256**, 63 (1996).

[49] M. Rosenblit and J. Jortner, Phys. Rev. Lett. **75**, 4079 (1995).

[50] G. D. Stein, Surf. Sci. **156**, 44 (1985).

[51] D. S. Peterka, A. Lindinger, L. Poisson, M. Ahmed, and D. M. Neumark, Phys. Rev. Lett. **91**, 043401 (2003).

[52] P. Claas, S. O. Mende, and F. Stienkemeier, Rev. Sci. Instrum. **74**, 4071 (2003).

[53] A. Golov and S. Sekatskii, Z. Phys. D: At., Mol. Clusters **27**, 349 (1993).